CHEMICAL ENGINEERING RESEARCH AND DESIGN XXX (2009) XXX–XXX

Contents lists available at ScienceDirect

Chemical Engineering Research and Design

journal homepage: www.elsevier.com/locate/cherd

Ekman pumping and intermittent particle resuspension in a stirred tank reactor

V. Lavezzo[a], R. Verzicco[c], A. Soldati[a,b,*]

[a] Dipartimento di Energetica e Macchine, Università degli Studi di Udine, via delle Scienze, 208 - 33100 Udine, Italy
[b] Centro Interdipartimentale di Fluidodinamica ed Idraulica, via Palladio, 8 - 33100 Udine, Italy
[c] Dipartimento di Ingegneria Meccanica, Università degli Studi di Roma "Tor Vergata", 00133 Roma, Italy

ABSTRACT

Lagrangian particle tracking and Direct Numerical Simulation of turbulence are used to highlight an intermittent phenomenon which is relevant for particle resuspension dynamics in an unbaffled tank reactor stirred by an eight blade paddle impeller. This phenomenon is associated with the Ekman pumping effect and its frequency scales in terms of the impeller rotation speed. We examine the dispersion of three swarms of heavy particles of different diameter demonstrating qualitative and quantitative features of the resuspension phenomenon.

Keywords: DNS; Mixing; Ekman pumping; Stirred Tank Reactor

1. Introduction

The dispersion process within a stirred vessel is extremely complex since it involves structures characterized by different length and time scales: (i) large scales, associated with impeller rotation and non-periodic fluctuations with episodic, bursting events often identified as macro-instabilities; (ii) small scales associated with turbulence. Flow motions characterized by these different scales contribute to energy transfer, dissipation and also to mixing of species and to dispersion of suspended particles. Understanding the mixing process inside a tank is of key importance for the optimization of processes, vessel design and product quality in a wide variety of industrial applications.

Specifically, unbaffled tanks are widely used in food and powder industry processes, since they provide higher mixing times necessary for the particles to be efficiently entrained and dispersed in the liquid medium. The presence of baffles would suppress the development of the vortex at the impeller shaft, thus preventing particles from sinking and floating in the liquid, as described in Glover and Fitzpatrick (2007).

Many investigations based on both experiments and numerical simulations have been performed to identify the mechanisms promoting the generation of the large-scale structures and to capture the particle interaction with large and small scales in baffled vessels. Ducci and Yianneskis (2007) employed a vortex tracking methodology to accurately investigate by means of PIV and LDA techniques, the precession of macro-instability (MI) vortices in stirred vessels. They demonstrated that the knowledge of the MI vortex path may reduce considerably the mixing time. Galletti et al. (2005) focused their analysis on the different types of instabilities that are present in most stirred tanks: precessional (MI) and impeller stream flow instabilities. They calculated the energy of such instabilities and showed that understanding their magnitude and frequency would provide methodologies for the design of more efficient operations. Nikiforaki et al. (2003) studied different vessel configurations by means of LDA and found that MI frequencies, related to the rotational speed velocity (N), are in the range of $0.015–0.02N$ (Hz) for high-Reynolds numbers and in the range of $0.04–0.15N$ for low Re. Comparisons between numerical simulations (Large Eddy Simulation, LES) and experiments have been performed by, e.g. Hartmann et al. (2004) and Roussinova et al. (2003) who calculated frequency and nature of the macro-instabilities.

In a previous work (Sbrizzai et al., 2006), we examined by means of Direct Numerical Simulation (DNS) the turbulent flow field in a flat-bottom unbaffled stirred tank equipped

* *Corresponding author at*: Dipartimento di Energetica e Macchine, Università degli Studi di Udine, via delle Scienze, 208 - 33100 Udine, Italy.
E-mail address: soldati@uniud.it (A. Soldati).
Received 3 October 2008; Received in revised form 12 December 2008; Accepted 5 January 2009
0263-8762/$ – see front matter © 2009 Published by Elsevier B.V. on behalf of The Institution of Chemical Engineers.
doi:10.1016/j.cherd.2009.01.004

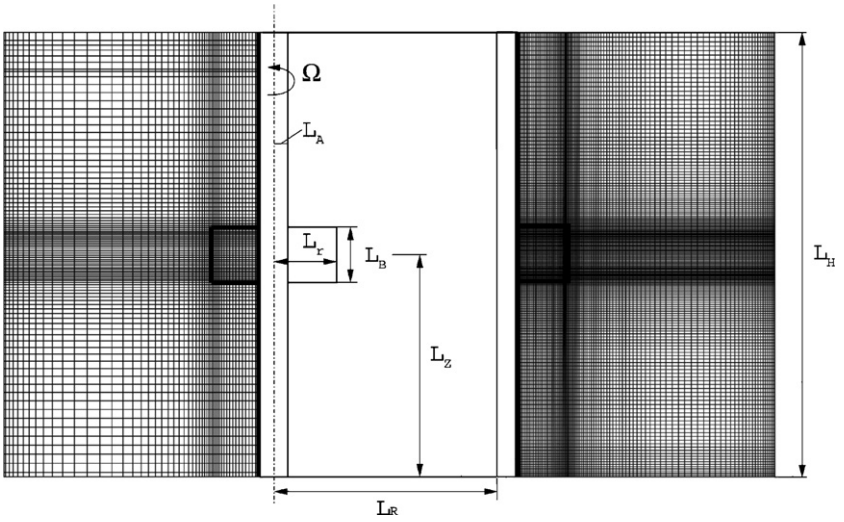

Fig. 1 – (Center) Vessel geometry, dimensions are made dimensionless using the impeller radius $L_r = 1.25$ cm: $L_r^* = 1$, $L_B^* = 0.8$, $L_A^* = 0.32$, $L_R^* = 4$, $L_Z^* = 4$ and $L_H^* = 8$; (left) computational grid used for flow field simulation (97 × 102 × 192 nodes in the azimuthal, radial and axial direction, respectively); (right) computational grid obtained by doubling the number of nodes in each direction (193 × 203 × 383 nodes in the azimuthal, radial and axial direction, respectively).

with an eight-blade paddle impeller. Lagrangian tracking of different size solid particles was exploited to analyze particle distribution in the vessel and identify high/low-dispersion regions.

Since in that work the simulation covered just *three* impeller revolutions, it was possible to show only the potential of the simulation. An advantage of the simulation was that we could examine the local particle distribution and we were able to show the scales of the local segregation patterns for particles of different size. Unfortunately, due to the brevity of the simulations, we could not investigate the long-term phenomena. This limit is overcome in the present work by extending the simulation time up to 21 impeller revolutions to establish some of the fundamental flow features of an unbaffled mixing tank.

During the entire simulation time, we tracked large swarms of particles characterized by different inertia. Inertial particles filter higher frequency turbulence motions, but respond quickly to large-scale motions. Thus, albeit low-fidelity for higher frequency, particles are natural tracers and by examining their motion it was possible to identify the presence of an intermittent vortex which wraps around the shaft in helical motion from the bottom of the tank to the impeller blades. This large-scale vortex finds its origin in the Ekman pumping effect and can be considered the main responsible for particle re-suspension in the vessel. Our findings have shown that the Ekman pumping can be associated to a precessional vortex type of macro-instability, but due to the absence of baffles a different effect on the flow is expected.

The objectives of this paper are (i) to characterize qualitatively the intermittent large-scale vortex and quantify its contribution to the re-suspension/dispersion of inertial particles, (ii) compare our findings with the results obtained in baffled tanks and (iii) to achieve a better insight on particle behavior by extending the simulation up to 21 revolutions.

We use the finite-difference second-order accurate code described in Verzicco et al. (2004) to solve the Navier–Stokes equations and the immersed-boundary approach (Fadlun et al., 2000) to model the impeller rotation. Dispersion of 30, 50 and 100 μm particles is simulated by means of Lagrangian tracking with a particle to fluid density ratio of 5.

2. Methodology

2.1. *Fluid flow*

The Navier–Stokes equations are solved in a cylindrical reference frame for the reactor geometry shown at the center of Fig. 1. Dimensions of vessel/impeller are made dimensionless using the impeller radius $L_r = 1.25$ cm: $L_r^* = 1$, $L_B^* = 0.8$, $L_A^* = 0.32$, $L_R^* = 4$, $L_Z^* = 4$ and $L_H^* = 8$. The impeller rotation velocity N is equal to 100 rpm or $\Omega = 10.47$ rad/s. Reference time-scale and velocity are the rotation time, $1/\Omega$, and the blade tip velocity, $U_T = \Omega L_r$. The working fluid is water, with density $\rho = 10^3$ kg/m^3 and kinematic viscosity $\nu = 10^{-6}$ m^2/s. The Reynolds number, based on the impeller blade and blade tip velocity, $Re = \Omega L_r^2/\nu$, is 1636. The imposed boundary conditions are (i) no-slip at impeller blades and at external walls (enforced using the immersed boundary method) and (ii) free-slip at the top surface to mimic the presence of a flat free surface between water and upper air. As estimated in Serra et al. (2001) and Verzicco et al. (2004), the free surface deformation is small and should not influence the overall (and local) evolution of the flow field justifying the assumption of a flat, stress-free upper boundary condition.

We started from the last flow field obtained in Sbrizzai et al. (2006) and we advanced the simulation in time up to 21 impeller revolutions. This was done with a grid resolution of $97 \times 102 \times 192$ grid points in the azimuthal, radial and axial direction, respectively. A benchmark grid obtained by doubling the number of grid nodes in each direction, totaling $193 \times 203 \times 383$ points in the azimuthal, radial and axial direction respectively has been used to assess the accuracy of the method (not discussed here). The turbulent kinetic energy and the energy dissipation rate have been used as parameters to compare the two grids. Since no evident difference has been found either in the impeller region or at the bottom of the tank between the two configurations, the coarse grid has been chosen for the whole simulation without applying further refinement, but in the regions where higher velocity gradients are expected (see the left and right sides of Fig. 1). Specifically, refinements are made in the blade region and

Please cite this article in press as: Lavezzo, V., et al., Ekman pumping and intermittent particle resuspension in a stirred tank reactor, Chem Eng Res Des (2009), doi:10.1016/j.cherd.2009.01.004

close to the shaft (see Sbrizzai et al., 2006 for a more detailed description).

As in Sbrizzai et al. (2006) we estimated the Kolmogorov length and time scales assuming that the relevant scales at which energy is introduced in the flow are the blade radius, L_r and the blade tip velocity, ΩL_r (Derksen, 2003) obtaining $\eta = Re^{-3/4} L_r = 48.5\,\mu m$ and $\tau = 1/\Omega\, Re^{-0.5} = 2.35 \times 10^{-3}$ s. These values have been used to assess the choice of space and time resolution by comparison with the minimum values of grid spacing: $L_A\,\Delta\theta = 259\,\mu m$, $\Delta r = 144\,\mu m$ and $\Delta z = 169\,\mu m$ which correspond to 5, 3 and 3.5 times the estimated Kolmogorov spatial scale, respectively. The time step used to advance the flow field calculation is $\Delta t = 1.25 \times 10^{-4}$ s, i.e. about 1/18 of the Kolmogorov time scale. This time constraint was imposed by particle simulation. We started our calculation from a developed turbulent flow in correspondence to the third impeller revolution, i.e. the last flow field obtained in our previous work.

Lagrangian tracking was performed for a time window corresponding to 18 impeller revolutions, starting from particle position and velocity reached at the end of the 3rd impeller revolution in our previous work, thus having a full investigation on particle behavior on 21 revolutions.

2.2. *Lagrangian tracking*

The methodology used for particle tracking is based on the same modeling and interpolation procedures used in a number of our previous works (Sbrizzai et al., 2006; Marchioli et

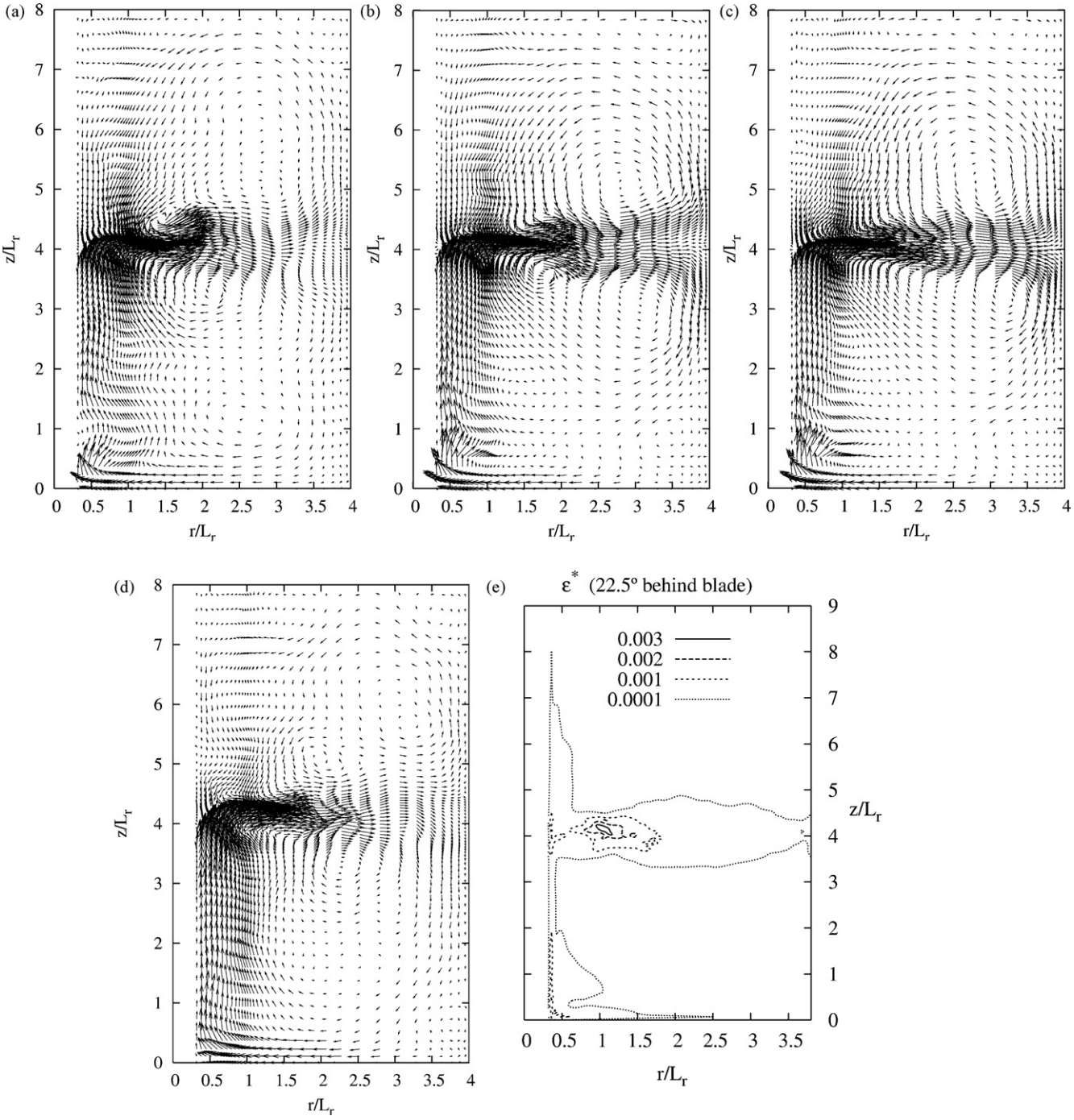

Fig. 2 – Instantaneous flow field of radial and axial velocity components on a vertical plane taken mid-way between two impeller blades after 3 (a), 9 (b), 15 (c) and 21 (d) impeller revolutions (one grid point every four is considered for visualization); (e) isocontours of turbulent energy dissipation on a meridional plane between two impeller blades.

Please cite this article in press as: Lavezzo, V., et al., Ekman pumping and intermittent particle resuspension in a stirred tank reactor, Chem Eng Res Des (2009), doi:10.1016/j.cherd.2009.01.004

al., 2007 among others). We report here the details and the assumptions for particle modeling, useful for the discussion on the results.

We simulate the dispersion of three swarms comprising O(10^4) solid particles of different diameter 30, 50 and 100 μm, with a density ratio with the fluid of $\rho_p/\rho = 5$. Particle density has been chosen quite high to stress the effect of inertia on particle behavior rather then to match a particular industrial application. According to many previous works (Biferale et al., 2005), since particles are small we chose the relevant flow time scale equal to the Kolmogorov time scale τ_k. The Stokes number, $St_k = \tau_p/\tau_k$, defined as the ratio between particle response time and a relevant flow time scale is in the range of [10^{-1} to 10^0].

The assumptions for particle modeling are: (i) all particles are point-wise, non-interacting, non-deformable solid spheres; (ii) particle density is large compared to fluid density; (iii) the effect of the particles on the flow is neglected; (iv) the particles do not collide with the impeller blades. Including other forces (lift, added mass, Basset force, etc.) and further complicative effects as collisions or two-way coupling might influence only the quantitative figures of particle dynamics and can be estimated of scarce importance for the objectives of this work (Picciotto et al., 2004). In accordance with these assumptions we calculate the trajectory of each particle by integrating explicitly over time the equation of motion which reduces to a balance of Stokes drag, gravity forces and particle inertia. The time resolution of the flow field was chosen equal to one half of the characteristic time scale of the smallest particle.

3. Results and discussion

The objectives of this section are: (i) to outline the main flow characteristics (ii) to comment on particle resuspension dynamics.

In Fig. 2 from (a) to (d), the instantaneous flow fields in a vertical section of the reactor taken midway between two impeller blades are shown. Vectors represent radial and axial velocity components in the plane. The flow fields shown in Fig. 2 are taken after 3, 9, 15 and 21 impeller revolutions, respectively. A characteristic flow pattern is clearly visible with a discharge jet issued radially from the impeller blade tip that splits in correspondence to the external wall, into two axial streams, upward and downward, respectively. These streams give rise to two main circulations having the shape of an upper and a lower toroidal vortex, respectively. Comparing Fig. 2 from (a) to (d) we may notice that the length of the discharge jet is oscillating in the radial direction during our simulation. After three impeller revolutions it is confined within $2L_r$ and low both radial and axial velocity components are observed at the wall. At intermediate times (Fig. 2(b) and (c)) high velocities are found in correspondence to the jet impingement at the wall. After 21 impeller revolutions, i.e. at the end of the simulation, the jet returns to be confined within $2L_r$ thus, closing a cycle. This behaviour is consistent with the results of Roussinova et al. (2004) who observed a low frequency, high-amplitude variation of the axial velocity in correspondence to both the impeller stream and the wall due to the presence of what they call a "circulation pattern" macro-instability. The radial jet extension is associated with a shift of the core of the two toroidal vortices toward the jet. The resultant position is in good agreement with that obtained in Dong et al. (1994) in their experiments with the circulation centers that lie at r/L_R equal to 0.75 and half way between the impeller and the liquid surface for the upper loop and about one quarter from the impeller for the lower loop. This confirms that a time longer than three impeller revolutions is required to visualize long-term phenomena, such as the discharge jet velocity variations, thus supporting our choice to extend the simulation and to produce this study.

3.1. *Ekman pumping*

After examining pictures and rendering of particle dynamics to explore their segregation patterns, we observed the presence of an intermittent precessional vortex that wraps around the shaft in rotating motion, from the bottom of the tank to the impeller blades. This is visible in Fig. 3(a). Instantaneous vorticity isocontours are used to identify the helical structure. Only a small cylinder below the impeller blades is considered for visualization. This large-scale structure finds its origin in the effect known as "Ekman pumping" which is caused by a convergence of fluid in the Ekman layer, i.e. the boundary layer in correspondence to the interface between a rotating flow and a solid boundary at which no-slip condition is applied and where viscous forces are of significant importance. This type of layer corresponds, in the present study, to the region at the bottom of the tank in the vicinity of the shaft. Here high values of energy dissipation rate ε^* are found, as visible in Fig. 2(e) where isocontours of ε^* for a meridional plane taken 22.5° behind the impeller blade, i.e. mid-way between two blades are shown (values are made dimensionless using $\varepsilon^* = \varepsilon/\Omega^3 L_r^2$)). The fluid, brought in a counter clock-wise circulation by the impeller rotating motion, is brought to a stop against the flat no-slip bottom of the vessel.

The thickness of the Ekman layer can be expressed as: $\delta = (\nu/\Omega)^{1/2} = 309$ μm, and it is characterized by the dimensionless parameter known as Ekman number E_k. This is similar to the inverse of the Reynolds number and represents essentially the ratio of viscous to Coriolis forces, defined as $E_k = \nu/\Omega L_r^2$, where ν is fluid kinematic viscosity, Ω the impeller rotation velocity and L_r the blade length taken as dimensional reference. If we consider the outer region, i.e. if we neglect the Ekman boundary layer, the Ekman number is smaller than unity (6.11×10^{-4}) indicating that the Coriolis forces dominate the fluid motion by balancing the radial pressure gradient created by the impeller jet and viscous forces are of negligible importance. In other words, the main motion is dominated by rotational rather than by frictional processes.

To get further insight into the role of these forces in the spin-up motion, we evaluated the time-scales involved in the process. A spin-up dominated by viscous forces will occur over a viscous time scale which is approximately: $t_v = L_H^2/\nu$ where L_H is the tank height and ν the kinematic viscosity of the fluid. A spin-up dominated by rotational forces will be similarly characterized by the Ekman time t_{E_k}, defined as $t_{E_k} = 1/(E_k^{1/2}\Omega)$) (Lim et al., 1993) where E_k is the Ekman number previously calculated. The value of the Ekman time is $t_{E_k} = 3.86$, whereas the viscous time t_v is 10^4. In this case, the fluid will take a time O(10^3) larger to spin-up if there were only viscous forces acting on it. It is straightforward to notice that Ekman mechanism dominates the spin-up of the fluid and enhances mass transport.

If we consider the Ekman vortex as a precessional vortex type of MI, it is well known from the literature (Nikiforaki et al., 2003; Galletti et al., 2005 among others) that one of the main effects of the macro-instabilities arising in a tank is to broaden

Please cite this article in press as: Lavezzo, V., et al., Ekman pumping and intermittent particle resuspension in a stirred tank reactor, Chem Eng Res Des (2009), doi:10.1016/j.cherd.2009.01.004

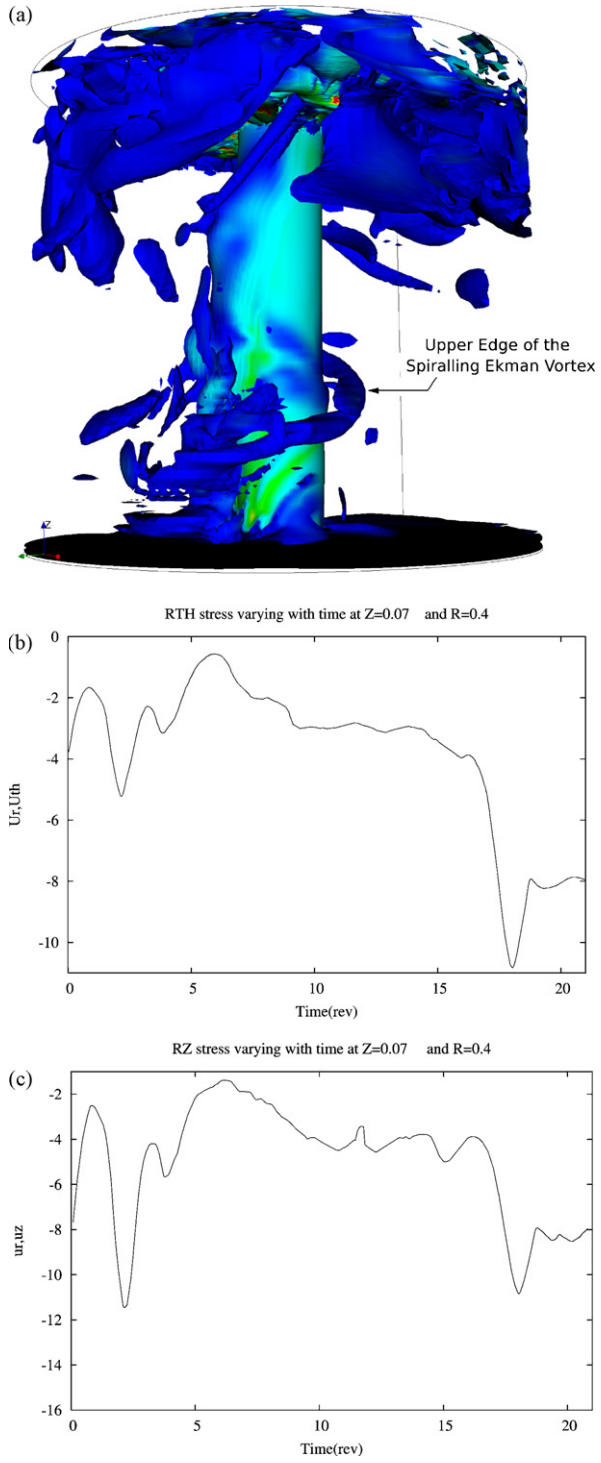

Fig. 3 – (a) Instantaneous vorticity isocontours after about six impeller revolutions. A cylinder of radius $2 \cdot L_r$ taken below the impeller blades is considered for visualization and Reynolds stresses calculated at $Z = 0.07L_r$ and $R = 0.4L_r$ in the r–θ direction (b) and (c) the r–z direction.

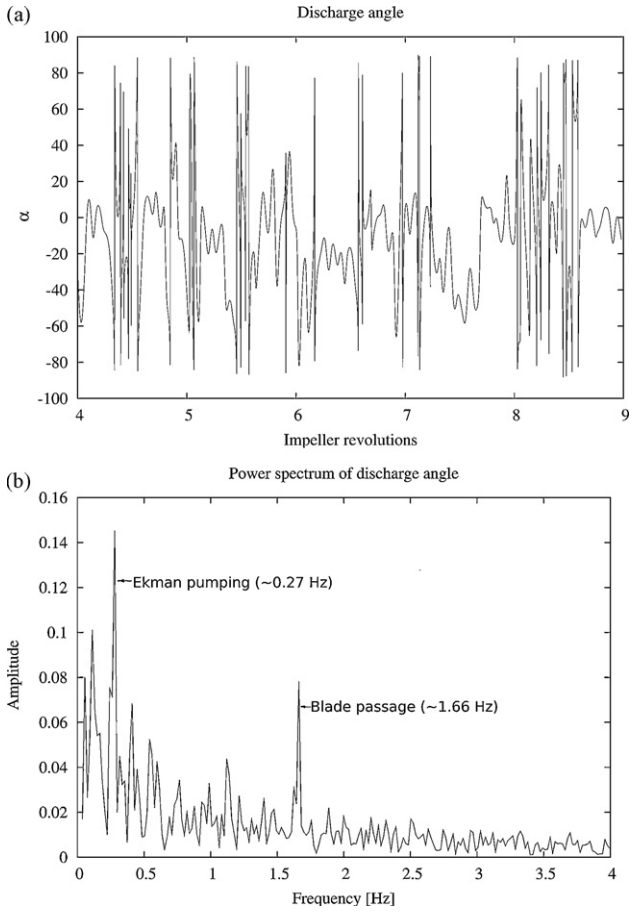

Fig. 4 – (a) Time-record of discharge angle of the impeller stream calculated as the ratio of the mean axial velocity component to the mean radial velocity component. Only five impeller revolutions are considered for visualization. (b) Power spectral density of the time record of the impeller jet discharge angle.

the turbulence level and enhance the level of mixing between the different species. In a turbulent flow field, as in the present case, the Reynolds stresses take place of the viscous stresses in the Ekman boundary layer, so that a change in the parameters and an effect on the flow is expected.

To this aim we calculated the time-record of the Reynolds stresses components in the r–θ and r–z directions. As shown in Fig. 3(b), a peak is reached in the r–θ direction every 5.8 impeller revolutions. The peaks are slightly shifted in time in the r–z direction, as visible in Fig. 3(c), since the vortex movement is mainly tangential at a first stage and acquires an axial component, due to convection, as time proceeds giving rise to the slight lag. The increase in the Reynolds stresses is responsible for an apparent increase in the effective viscosity of the fundamental flow. This produces an increase in the Ekman number, and consequently a reduction in the Ekman time. In light of this, when the Ekman pumping becomes effective the transport of mass to the impeller blades becomes faster and the spin-up of the fluid is enhanced, giving rise to the helical motion previously described. From the results of our numerical simulation, we observed that the Ekman pumping is characterized by a specific dimensionless frequency ($f' = 60f/N = 0.162$, where N is the impeller speed expressed in rpm).

When the circulation flow in the lower part of the vessel becomes more energetic a change in the discharge angle of the impeller stream is observed. The angle has been evaluated as the ratio of the spatially averaged axial velocity to the spatially averaged radial velocity calculated over an area in correspondence to one of the blade tip (Fan et al., 2004). The time record is shown in Fig. 4(a). To further investigate the records of the discharge angle, the power spectral density has been calculated considering the entire simulation time-span, as visible in Fig. 4(b). We can notice the presence of two high

Please cite this article in press as: Lavezzo, V., et al., Ekman pumping and intermittent particle resuspension in a stirred tank reactor, Chem Eng Res Des (2009), doi:10.1016/j.cherd.2009.01.004

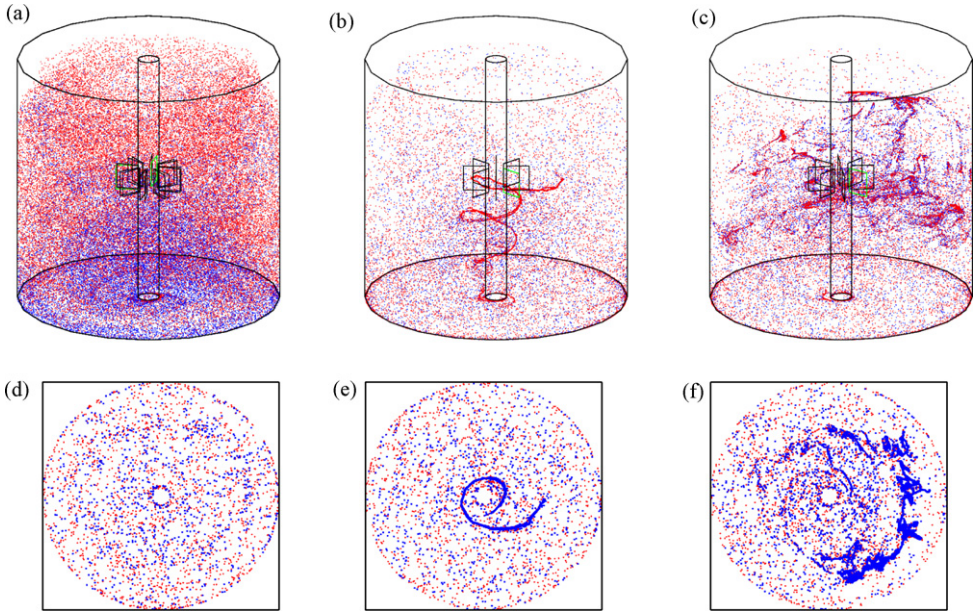

Fig. 5 – Snapshots of instantaneous particle position considering the entire vessel and a horizontal thin slice taken in correspondence to the mid-plane of the tank, for 100 μm particles. The instants at 3 (a and d), 6.5 (b and e) and 7.3 (c and f) impeller revolutions are considered for visualization.

peaks, one in correspondence to the blade passage (~1.66 Hz) and one in correspondence to 0.27 Hz. This latter corresponds to a low-frequency fluctuation of the signal referred to as the macro-instability frequency. This frequency can be associated, in the present study, to the Ekman pumping effect, giving the aforementioned dimensionless value of $f' = 0.162$. This value differs slightly from the results obtained by Nikiforaki et al. (2003) who found a frequency range of $0.04 < f' < 0.15$. The reasons for this discrepancy may be: (i) the different geometry employed in that study, a baffled tank, with respect to the unbaffled tank of the present work and (ii) the different Reynolds number which is lower in our case. This results might be a confirmation on the similarities between the MI and the Ekman pumping effect and might be useful for a better

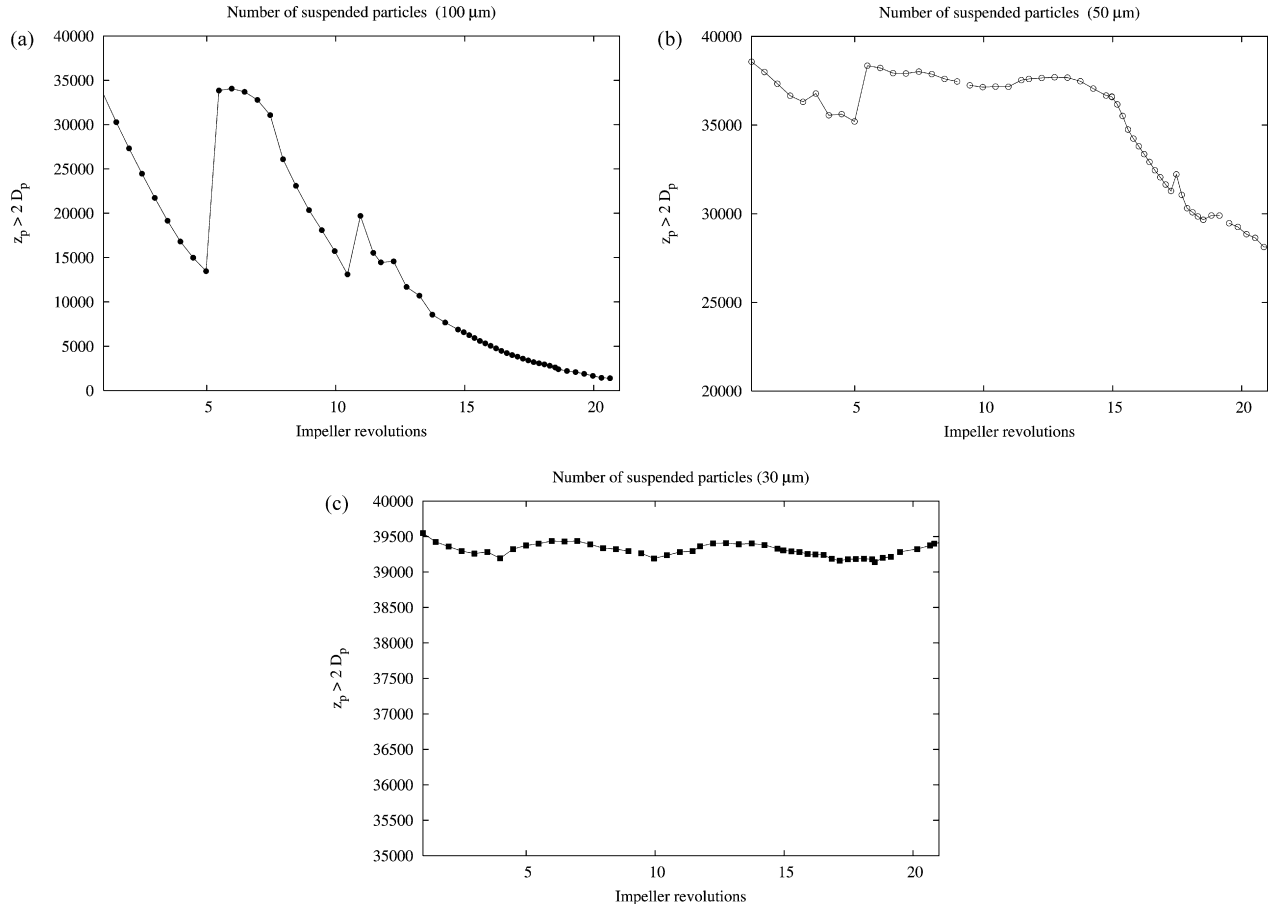

Fig. 6 – Number of suspended particles in the vessel varying with time for 100 μm (a), 50 μm (b) and 30 μm (c) particles.

Please cite this article in press as: Lavezzo, V., et al., Ekman pumping and intermittent particle resuspension in a stirred tank reactor, Chem Eng Res Des (2009), doi:10.1016/j.cherd.2009.01.004

understanding on the physics underlying the two configurations, but further investigations are still necessary.

This pumping effect is more evident if we observe the behavior of particles dispersed in the fluid. We started our calculation from the particle position and velocity obtained at the end of the third impeller revolution considering two swarms of 2×10^4 particles for each diameter (30, 50 and 100 μm), distributed at random in the vessel. To get insights on the influence of the injection point on the dispersion and settling process, half of the particles have been released above the impeller plane ($z = L_H/2$) and half in the lower part of the tank. Red particles are those released in the upper half of the vessel, blue particles those released in the lower half. Observing a full time-dependent animation of the motion of particle swarms is very instructive on the physics of the phenomena. In Fig. 5, we show some motion-capture snapshots of the dynamics of particles for the 100 μm swarm. Due to their stronger gravitational settling, larger particles collect faster at the bottom of the tank, where, due to the concentric sweeping effect of the Ekman layer, particles are accumulated around the shaft. When the spiralling vortex bursts out of the Ekman layer, many particles are swept upwards. This phenomenon occurs for all particles, but is more evident in our simulation relative to 100 μm particles. We choose three instants of the simulation which can tell the story of particle re-suspension. A perspective view of the whole tank and a top-view considering a thin slice in correspondence to the impeller blades after 3 (a and d), 6.5 (b and e) and 7.3 (c and f) impeller revolutions are shown in Fig. 5. At the beginning particles show no preferential distribution. Perhaps, a slightly visible spiralling pattern is observable at the bottom of the tank (Fig. 5(a)). The action of the spiralling vortex is clearly visible after 6.5 revolutions. Particles have been entrained and clearly mark the upper edge of the vortex. The upper tip of the vortex has approached the blade height and is about to intersect with the radial jet (see also Fig. 2). After almost seven revolutions, all the particles entrained by the vortex have been dispersed by the action of the impeller blades. A rather, macroscopically homogeneous particle distribution is obtained. Locally, preferential particle patterns are visible: these are still under the influence of some coherent portions of the vortex which was destroyed by the blades radial jet. During the course of our simulation the spiralling vortex occurred trice together with intense particle re-suspension.

In Fig. 6, we show the evolution of the number of suspended particles over time (measured in impeller revolutions). A particle is considered suspended when its distance from the bottom wall is greater than twice the particle diameter. Larger 100 μm particles (Fig. 6(a)) show a sharp gradient in correspondence to second half of the fifth revolution and a minor one in correspondence to almost half of the 11th. It is possible to observe that after the 12th revolution the number of suspended particles is continuously decreasing. This is due to the fact that all the particles are collecting in the viscous layer at the bottom of the tank due to both gravity and their inertia and therefore the fluid is not longer able to suspend them into the fluid. The effect of the spiralling vortex is more moderate for the medium size, 50 μm particles (Fig. 6(b)) at an initial stage, but it becomes more effective as time proceeds and a larger number of particles enters the Ekman layer due to gravitational effects. A peak in correspondence to half of the 17th revolution is, indeed, visible, thus confirming the frequency of the vortex previously found. Re-suspension mechanisms due to Ekman pumping spiralling vortex are slightly noticeable for the smaller 30 μm particles (Fig. 6(c)) which exhibit only a wavy behaviour throughout the simulation. This result confirms the importance the Ekman vortex has, in particle to fluid mixing and particle re-suspension in the tank expecially for particles entrained in the Ekman layer.

4. Conclusions

In this work we investigated the dispersion of small solid particles in a stirred tank using a DNS code to solve the flow balance equations down to the smallest scales (i.e. the Kolmogorov scales) and a Lagrangian approach to simulate the behavior of three swarms of 30, 50 and 100 μm particles dispersed in the vessel. We started our calculation from the developed turbulent flow field and particle position and velocity obtained at the end of the previous work (Sbrizzai et al., 2006) extending the simulation up to 21 impeller revolutions.

The velocity field shows a characteristic flow pattern with the presence of an intermittent Ekman pumping which appears twice during the simulation. The impeller discharge angle and the Reynolds stress components have been used to calculate the frequency of the spiralling vortex obtaining a value of $f' = 0.162$.

A time-dependent animation of the motion of the particles dispersed in the vessel has put into evidence that particles tend to accumulate at the bottom of the tank due to gravitational effects, depending on their inertia, and to be driven close to the shaft by a concentric sweeping flow. This phenomenon continues until the Ekman pumping becomes effective and a large spiralling vortex entrains and drives particles into a long filament to the impeller blades. Here, the radial jet issued from the impeller is responsible for particle re-dispersion in the vessel. The spiralling vortex is associated with a strong particle re-suspension. This phenomenon, more evident for larger 100 μm particles, occurs for all swarms after about 6, 11 and 17 impeller revolutions.

References

Biferale, L., Boffetta, G., Celani, A., Lanotte, A. and Toschi, F., 2005, Particle trapping in three dimensional fully developed turbulence. Phys Fluids, 17: 021701.

Derksen, J.J., 2003, Numerical simulation of solids suspension in a stirred tank. AIChE J, 49(11): 2700–2714.

Dong, L., Johansen, S.T. and Engh, T.A., 1994, Flow induced by an impeller in an unbaffled tank-I. Experimental. Chem Eng Sci, 49: 549–560.

Ducci, A. and Yianneskis, M., 2007, Vortex tracking and mixing enhancement in stirred processes. AIChE J, 53: 305–315.

Fadlun, E.A., Verzicco, R., Orlandi, P. and Mohd-Yusof, J., 2000, Combined immersed boundary/finite-difference methods for three-dimensional complex flow simulations. J Comp Phys, 161: 35–60.

Fan, J., Wang, Y., Rao, Q. and Fei, W., 2004, A study on intermittency phenomena in the impeller stream via digital particle image velocimetry (DPIV). Chem Eng Sci, 102: 25–33.

Galletti, C., Paglianti, A. and Yianneskis, M., 2005, Observations on the significance of instabilities turbulence and intermittent motions on fluid mixing processes in stirred reactors. Chem Eng Sci, 60: 2317–2331.

Glover and Fitzpatrick., 2007, Modelling vortex formation in an unbaffled stirred tank reactors. Chem Eng J, 127: 11–22.

Hartmann, H., Derksen, J.J. and van den Akker, H.E.A., 2004, Macroinstability uncovered in a Rushton turbine stirred tank by means of LES. AIChE J, 50: 2383–2393.

Lim, T.G., Choi, S. and Hyun, M.J., 1993, Transient interface shape of a two-layer liquid in an abruptly rotating cylinder. J Fluids Eng, 115(2): 324–329.

Please cite this article in press as: Lavezzo, V., et al., Ekman pumping and intermittent particle resuspension in a stirred tank reactor, Chem Eng Res Des (2009), doi:10.1016/j.cherd.2009.01.004

Marchioli, C., Picciotto, M. and Soldati, A., 2007, Influence of gravity and lift on particle velocity statistics and transfer rates in turbulent vertical channel flow. Int J Multiphase Flow, 33: 227–251.

Nikiforaki, L., Montante, G., Lee, K.C. and Yianneskis, M., 2003, On the origin, frequency and magnitude of macro-instabilities of the flows in stirred vessels. Chem Eng Sci, 58: 2937–2949.

Picciotto, M., Giusti, A., Marchioli, C. and Soldati, A., 2004, Turbulence modulation by micro-particles in boundary layers, in Proceedings of IUTAM Symposium on Computational Approaches to Multiphase Flow (Springer).

Roussinova, V., Kresta, S.M. and Weetman, R., 2003, Low frequency macroinstabilities in a stirred tank: scale-up and prediction based on large eddy simulations. Chem Eng Sci, 58: 2297–2311.

Roussinova, V.T., Kresta, S.M. and Weetman, R., 2004, Resonant geometries for circulation pattern macroinstabilities in a stirred tank. AIChE J, 50: 2986–3005.

Sbrizzai, F., Lavezzo, V., Verzicco, R., Campolo, M. and Soldati, A., 2006, Direct numerical simulation of turbulent particle dispersion in an unbaffled stirred-tank reactor. Chem Eng Sci, 61: 2843–2853.

Serra, A., Campolo, M. and Soldati, A., 2001, Time dependent finite-volume simulation of the turbulent flow in a free-surface CSTR. Chem Eng Sci, 56: 2715–2720.

Verzicco, R., Fatica, M., Iaccarino, G. and Orlandi, P., 2004, Flow in an impeller-stirred tank using an immersed-boundary method. AIChE J, 50(6): 1109–1118.

Please cite this article in press as: Lavezzo, V., et al., Ekman pumping and intermittent particle resuspension in a stirred tank reactor, Chem Eng Res Des (2009), doi:10.1016/j.cherd.2009.01.004